Dalton Transactions

Accepted Manuscript

ROYAL SOCIETY OF CHEMISTRY

www.rsc.org/dalton

Narrowing the gap: From semiconductor to semimetal in the homologous series of rare-earth zinc arsenides $RE_{2-y}Zn_4As_4 \cdot n(RE\text{As})$ and Mn-substituted derivatives $RE_{2-y}Mn_xZn_{4-x}As_4 \cdot n(RE\text{As})$ (RE = La–Nd, Sm, Gd)†

Xinsong Lin, Danisa Tabassum, and Arthur Mar*

Department of Chemistry, University of Alberta, Edmonton, Alberta, Canada T6G 2G2

* *Department of Chemistry, University of Alberta, Edmonton, Alberta, Canada T6G 2G2. E-mail: arthur.mar@ualberta.ca; Fax: +1-780-492-8231*

† Electronic supplementary information (ESI) available: EDX analyses, complete crystallographic data, and powder XRD patterns. See DOI: 10.1039/xxxxxxxx

Abstract

A homologous series of ternary rare-earth zinc arsenides, prepared by reactions of the elements at 750 °C, has been identified with the formula $RE_{2-y}Zn_4As_4{\cdot}n(RE\text{As})$ (n = 2, 3, 4) for various *RE* members. They adopt trigonal structures: $RE_{4-y}Zn_4As_6$ (*RE* = La–Nd), space group $R\bar{3}m1$, Z = 3; $RE_{5-y}Zn_4As_7$ (*RE* = Pr, Nd, Sm, Gd), space group $P\bar{3}m1$, Z = 1; $RE_{6-y}Zn_4As_8$ (*RE* = La–Nd, Sm, Gd), space group $R\bar{3}m1$, Z = 3. The Zn atoms can be partially substituted by Mn atoms, resulting in quaternary derivatives $RE_{2-y}Mn_xZn_{4-x}As_4{\cdot}n(RE\text{As})$. Single-crystal structures were determined for nine ternary and quaternary arsenides $RE_{2-y}M_4As_4{\cdot}n(RE\text{As})$ (M = Mn, Zn) as representative examples of these series. The structures are built by stacking close-packed nets of As atoms, sometimes in very long sequences, with *RE* atoms occupying octahedral sites and *M* atoms occupying tetrahedral sites, resulting in an intergrowth of [*RE*As] and [M_2As_2] slabs. The recurring feature of all members of the homologous series is a sandwich of [M_2As_2]–[*RE*As]–[M_2As_2] slabs, while rocksalt-type blocks of [*RE*As] increase in thickness between these sandwiches with higher n. Similar to the previously known related homologous series $REM_{2-x}As_2{\cdot}n(RE\text{As})$ which is deficient in *M*, this new series $RE_{2-y}M_4As_4{\cdot}n(RE\text{As})$ exhibits deficiencies in *RE* to reduce the electron excess that would be present in the fully stoichiometric formulas. Enthalpic and entropic factors are considered to account for the differences in site deficiencies in these two homologous series. Band structure calculations indicate that the semiconducting behaviour of the parent n = 0 member (with $CaAl_2Si_2$-type structure) gradually evolves, through a narrowing of the gap between valence and conduction bands, to semimetallic behaviour as the number of [*RE*As] blocks increases, to the limit of $n = \infty$ for rocksalt-type *RE*As.

Keywords: Rare earths; Arsenides; Crystal structure; Site deficiencies; Electronic structure

Introduction

The ambitious goal for synthetic chemists to "design" new compounds with tunable properties must be tempered with the understanding that there are a limited number of experimental parameters under control and constraints on what is allowed by thermodynamic requirements.[1] Within these limitations, the idea of a homologous series does provide a convenient framework to systematize closely related compounds and to predict the existence of new members. In solid state chemistry, for example, many layered structures built up by stacking different types and numbers of slabs can be defined in terms of such homologous series and are found among oxides, chalcogenides, pnictides, and intermetallic compounds.[2–6] More complicated frameworks can be constructed through the condensation of modules or blocks of different sizes and shapes.[7–9] Of practical consequence, the physical and chemical properties are expected to vary gradually among members of a given homologous series; superconductivity and magnetic ordering are two examples of applications where small changes in crystal structure can have profound influence on properties.[10–12]

As part of an ongoing program to characterize ternary rare-earth transition-metal arsenides, which are of interest for their electrical and magnetic properties, investigations of *RE*–Zn–As systems have revealed many new phases: $RE\mathrm{Zn}_{0.67}\mathrm{As}_2$ (*RE* = La–Nd, Sm),[13,14] $RE_{0.67}\mathrm{Zn}_2\mathrm{As}_2$ (*RE* = La–Nd, Sm),[15] $RE\mathrm{Zn}_3\mathrm{As}_3$ (*RE* = La–Nd, Sm),[16] $RE\mathrm{Zn}_2\mathrm{As}_3$ (*RE* = La–Pr),[17] $RE\mathrm{Zn}_{2-x}\mathrm{As}_2{\cdot}n(RE\mathrm{As})$ (*RE* = La–Nd, Sm; *n* = 3, 4, 5, 6),[18] $RE\mathrm{Zn}_2\mathrm{As}_2$ (*RE* = Eu, Yb),[19–21] $\mathrm{Eu}_2\mathrm{Zn}_2\mathrm{As}_3$,[22] and $\mathrm{Eu}_{11}\mathrm{Zn}_6\mathrm{As}_{12}$.[23] Except for $\mathrm{LaZn}_3\mathrm{As}_3$ and $\mathrm{Eu}_{11}\mathrm{Zn}_6\mathrm{As}_{12}$, all of these compounds adopt structures derived by stacking Zn–As slabs in different sequences. The clearest manifestation of a homologous series is seen in $RE\mathrm{Zn}_{2-x}\mathrm{As}_2{\cdot}n(RE\mathrm{As})$, for which successive members (*n* = 3, 4, 5, 6) have trigonal structures built up by intergrowing [*RE*As] slabs of

increasing thickness between zinc-deficient [Zn_2As_2] slabs.[18] In fact, $RE Zn_2As_2$ or the rare-earth-deficient $RE_{0.67}Zn_2As_2$ can be considered to be the parent member (n = 0) of this series.[15,19–21] As n increases, the electronic structure evolves from a small band-gap semiconductor to a semimetal. A parallel but less extensive homologous series of tetragonal structures with the general formula $RE_2As_3{\cdot}n(Zn_{2-x}As)$ can be expressed for $RE Zn_{0.67}As_2$ (n = 1) and $RE Zn_2As_3$ (n = 3), in which successive members exhibit increasingly thicker Zn-containing slabs.[13,14,17] Exploiting the richness of these *RE*–Zn–As systems and extending the emerging structural patterns observed, we posit that other homologous series can be prepared with different stacking sequences and thereby expand on our ability to control the electronic structure. There is also growing evidence that Mn can successfully substitute for Zn in these and related compounds,[24] which could impart interesting magnetic properties.

Through the directed synthesis of deliberately targeted compositions, three new series of ternary arsenides $RE_{4-y}Zn_4As_6$ (*RE* = La–Nd), $RE_{5-y}Zn_4As_7$ (*RE* = Pr, Nd, Sm, Gd), and $RE_{6-y}Zn_4As_8$ (*RE* = La–Nd, Sm, Gd) have now been prepared, revealing the evolution of a different homologous series $RE_{2-y}Zn_4As_4{\cdot}n(RE As)$ (n = 2, 3, 4) which is rare-earth-deficient instead of zinc-deficient. Quaternary arsenides $RE_{2-y}Mn_xZn_{4-x}As_4{\cdot}n(RE As)$ in which Mn partially substitutes for Zn were also prepared. We attempt to understand the nature of *RE* deficiencies in these compounds through entropy considerations, and examine the bonding and electronic structure through band structure calculations.

Experimental

Synthesis

Starting materials were freshly filed *RE* pieces (99.9%, Hefa), Mn powder (99.6%, Alfa-Aesar), Zn shot (99.99%, Aldrich), and As lumps (99.999%, Alfa-Aesar). The ternary arsenides were initially identified in the course of preliminary syntheses with various loading compositions. After the chemical compositions were established, including the occurrence of *RE* deficiencies, the loading compositions $RE_{3.3}Zn_4As_6$, $RE_{4.3}Zn_4As_7$, and $RE_{5.3}Zn_4As_8$ were systematically prepared from mixtures of the elements on a 0.3-g scale for a broad range of trivalent *RE* components (La–Nd, Sm, Gd and beyond). The mixtures were loaded into fused-silica tubes, which were evacuated and sealed. The tubes were heated at 500 ºC for 2 d, heated to 750 ºC over 20 h, held at this temperature for 7 d, and then cooled to room temperature over 2 d. The volatility of Zn and As poses a major problem in the synthesis of ternary *RE*–Zn–As phases in general; the preheating step at 500 ºC helps minimize, but does not completely eliminate, loss of these components through sublimation. The existence of many competing phases with similar compositions, such as $RE Zn_{0.67}As_2$,[14] also makes phase-pure samples difficult to obtain, as evaluated from powder X-ray diffraction (XRD) patterns collected on an Inel diffractometer equipped with a curved position-sensitive detector (CPS 120) and a Cu $K\alpha_1$ radiation source operated at 40 kV and 20 mA (Figs. S1–S3 in ESI†). Substitution tends to be limited to the earlier *RE* components ($RE_{4-y}Zn_4As_6$ (*RE* = La–Nd), $RE_{5-y}Zn_4As_7$ (*RE* = Pr, Nd, Sm, Gd), $RE_{6-y}Zn_4As_8$ (*RE* = La–Nd, Sm, Gd)) and further substitution beyond Gd was unsuccessful. Unit cell parameters refined from the powder XRD patterns are listed in Table 1. In separate experiments intended to investigate transition-metal substitution in the different arsenides $RE Zn_3As_3$,[16] we had obtained quaternary phases $RE_{4-y}Mn_xZn_{4-x}As_6$ (*RE* = Ce, Nd) which were subsequently recognized to belong to one of the three homologous series described above. Further attempts in

Mn substitution within the other series resulted in two more examples, $RE_{6-y}Mn_xZn_{4-x}As_8$ (*RE* = Sm, Gd).

Crystals used for structure determination were obtained through further heat treatment at higher temperatures with the aim of exceeding melting points. The samples prepared above were reheated at 800 ºC for 2 d, heated to 1050 ºC over 20 h, held at this temperature for 7 d, slowly cooled to 500 ºC at a rate of 3 ºC/h, and cooled to room temperature over 2 d. Small crystals (constituting about 30% of the product) obtained from these reactions were examined on a JEOL JSM-6010LA scanning electron microscope and their compositions were determined by energy-dispersive X-ray (EDX) analyses on several points of individual crystals with acquisition times of 30 s each (Table S1 in ESI†). In general, the experimental compositions agree well with expectations. The crystals were unfortunately too small (typically 0.1 mm in longest dimension) to permit physical property measurements such as electrical resistivity.

Structure determination

Single crystals of ternary arsenides and some quaternary Mn-containing derivatives, whose chemical compositions were determined by EDX analyses, were mounted on a Bruker PLATFORM diffractometer equipped with a SMART APEX II CCD area detector and a graphite-monochromated Mo *K*α radiation source. Intensity data were collected at room temperature using ω scans in 5–8 batches at different ϕ angles with a frame width of 0.3º and an exposure time of 12–15 s per frame. Face-indexed numerical absorption corrections were applied. Structure solution and refinement were carried out with use of the SHELXTL (version 6.12) program package.[25] Atom positions and labels were standardized with the program STRUCTURE TIDY.[26]

Within the $RE_{4-y}Mn_xZn_{4-x}As_6$ series, crystals of an all-Zn ($Pr_{4-y}Zn_4As_6$) and two Mn-doped members ($Ce_{4-y}Mn_xZn_{4-x}As_6$, $Nd_{4-y}Mn_xZn_{4-x}As_6$) were available. Intensity symmetry and statistics indicated the centrosymmetric trigonal space group $R\bar{3}m1$. For $Pr_{4-y}Zn_4As_6$, the locations of three Pr, two Zn, and three As sites were initially found by direct methods. After refinement of this model, the displacement parameters for the Pr2 site were found to be much larger (U_{eq} = 0.04 Å^2) than for the Pr1 and Pr3 sites (U_{eq} = 0.01 Å^2). When the occupancies of these sites were freed, the refinements confirmed that the Pr2 site is partially occupied (~0.5) and now has more reasonable displacement parameters (U_{eq} = 0.01 Å^2), whereas the Pr1 and Pr3 sites remained fully occupied (1.0). At this stage, the difference Fourier map revealed considerable residual electron density of 12 e$^-$/Å^3 at 0, 0, 0.15, about 1.3 Å away from the existing Zn1 site at 0, 0, 0.13. This was assigned to be a secondary site, labeled Zn1b, while the original primary site was relabeled Zn1a. Refinements were performed in which these split sites were fixed to have equal displacement parameters and their occupancies were constrained to sum to unity. The occupancies converged to 0.9 Zn for the primary site (Zn1a) and 0.1 Zn for the secondary site (Zn1b). The other Zn site (Zn2) was well-behaved and unsplit. The difference map was now clean and the formula was determined to be $Pr_{3.46(1)}Zn_4As_6$, in reasonable agreement with the EDX analysis. For the Mn-doped compounds $Ce_{4-y}Mn_xZn_{4-x}As_6$ and $Nd_{4-y}Mn_xZn_{4-x}As_6$, similar features of partially occupied *RE* sites and split Mn/Zn sites were encountered, but the distribution of Mn and Zn atoms within the metal sites (labeled *M*1a/*M*1b and *M*2) must be considered carefully. The closely spaced *M*1a and *M*1b sites were each allowed to be occupied by a mixture of Mn and Zn atoms, with the constraint that the occupancies sum to unity. Given the large number of free parameters, the refinements were unstable but tended towards high occupancy of Zn in the *M*1a site and of Mn in the the *M*1b site. Based on this observation, we

applied a simplified structural model in which the *M*1a site is occupied exclusively by Zn atoms and the *M*1b site by Mn atoms; simultaneously, a mixture of Mn and Zn atoms can be accomodated within the unsplit *M*2 site. Refinements of this model led to the formulas $Ce_{3.32(1)}Mn_{1.1(1)}Zn_{2.9(1)}As_6$ and $Nd_{3.34(1)}Mn_{0.92(6)}Zn_{3.08(6)}As_6$.

Within the $RE_{5-y}Zn_4As_7$ series, crystals of the Nd and Sm members were available. Their structures were solved in the trigonal space group $P\bar{3}m1$. From similar observations as above, it was determined that the *RE*3 site is partially occupied (~0.4) and there is a set of split (Zn1a/Zn1b) and unsplit (Zn2) metal sites. Refinements following the procedure above led to the formulas $Nd_{4.41(1)}Zn_4As_7$ and $Sm_{4.39(1)}Zn_4As_7$.

Within the $RE_{6-y}Mn_xZn_{4-x}As_8$ series, crystals of two all-Zn ($Nd_{6-y}Zn_4As_8$, $Sm_{6-y}Zn_4As_8$) and two Mn-doped members ($Sm_{6-y}Mn_xZn_{4-x}As_8$, $Gd_{6-y}Mn_xZn_{4-x}As_8$) were available. Their structures were solved in the trigonal space group $R\bar{3}m1$. The *RE*3 site is partially occupied (0.3–0.4) and the metal sites are *M*1 and *M*2a/*M*2b. The $Sm_{6-y}Mn_xZn_{4-x}As_8$ structure provides an example in which the site preferences of Mn and Zn within the split metal sites were clearly revealed from intermediate refinements which led to occupancies of 0.7 Zn / –0.1 Mn in the *M*2a site and –0.1 Zn / 0.5 Mn in the *M*2b site. The structural model was then simplified to *M*2a containing only Zn and *M*2b containing only Mn. Because the unsplit *M*1 site showed a strong preference to be occupied by Zn atoms (0.9 Zn / 0.1 Mn), we chose to assign this site to contain exclusively Zn atoms. Final refinements led to the formulas $Nd_{5.43(1)}Zn_4As_8$, $Sm_{5.40(1)}Zn_4As_8$, $Sm_{5.33(1)}Mn_{0.58(1)}Zn_{3.42(1)}As_8$, and $Gd_{5.27(1)}Mn_{0.62(1)}Zn_{3.38(1)}As_8$.

In general, the structure refinements led to excellent agreement factors (conventional *R*(*F*) values ranging from 0.02 to 0.04) and featureless difference maps ($(\Delta\rho)_{max}$, $(\Delta\rho)_{min}$ values around 4 and –4 e/Å^3, respectively). Full experimental details (crystallographic data, positional

and displacement parameters, interatomic distances) are given in Tables S2–S4 in ESI†. Abbreviated crystallographic data are listed in Table 2 and selected ranges of interatomic distances are listed in Table 3. Further data, in CIF format, have been sent to Fachinformationszentrum Karlsruhe, Abt. PROKA, 76344 Eggenstein-Leopoldshafen, Germany, as supplementary material No. CSD-430205 to 430213 and can be obtained by contacting FIZ (quoting the article details and the corresponding CSD numbers).

Band structure calculations

Tight-binding linear muffin tin orbital band structure calculations were performed within the local density and atomic spheres approximation with use of the Stuttgart TB-LMTO-ASA program (version 4.7).[27] Fully stoichiometric models were constructed for the series $La_2Zn_4As_4 \cdot n(LaAs)$ with n = 0, 1, 2, 3, 4, 5, and ∞. Cell parameters and atomic positions were taken from single-crystal structure determinations where these were available, in which the *RE* component was replaced by La to avoid computational problems associated with filled f orbitals. The calculations for $La_2Zn_4As_4$ (n = 0, based on the $CaAl_2Si_2$-type structure of $Ce_{0.63}Zn_2As_2$)[15] and LaAs (n = ∞, based on the rocksalt-type structure in space group $Fm\bar{3}m$ with a = 6.16 Å)[28,29] reproduce results reported previously[18] and are included here for comparison. For the hypothetical compounds $La_3Zn_4As_5$ (n = 1) and $La_7Zn_4As_9$ (n = 5), the cell parameters were extrapolated from the trends followed by the real compounds (n = 0, 2, 3, 4) and the atomic positions were chosen to give La–As bonds of 3.0 Å and Zn–As bonds of 2.5–2.6 Å, similar to those found in the real compounds. The basis set consisted of La 6s/6p/5d/4f, Zn 4s/4p/3d, and As 4s/4p/4d orbitals, with the La 6p and As 4d orbitals being downfolded. Integrations in reciprocal space were carried out with an improved tetrahedron method over 131 irreducible k

points within the first Brillouin zone from a 12 × 12 × 8 mesh for those structures in space group $P\bar{3}m1$, or over 189 irreducible *k* points from a 12 × 12 × 12 mesh for those structures in space group $R\bar{3}m1$.

Results and discussion

The new ternary arsenides $RE_{4-y}Zn_4As_6$ (*RE* = La–Nd), $RE_{5-y}Zn_4As_7$ (*RE* = Pr, Nd, Sm, Gd), and $RE_{6-y}Zn_4As_8$ (*RE* = La–Nd, Sm, Gd) belong to a homologous series with the general formula $RE_{2-y}Zn_4As_4 \cdot n(RE\text{As})$ (n = 2, 3, 4), which joins the previously known series $RE\text{Zn}_{2-x}\text{As}_2 \cdot n(RE\text{As})$ (n = 3, 4, 5, 6)[18] to form two daughter branches of an emerging family of trigonal structures that share $RE_{2-y}Zn_4As_4$ (represented by $RE_{0.67}Zn_2As_2$ (*RE* = La–Nd, Sm)[15] or $RE\text{Zn}_2\text{As}_2$ (*RE* = Eu, Yb)[19–21]) as the parent n = 0 member. In all of these phases, Mn atoms can partially substitute for Zn atoms, resulting in the quaternary arsenides $RE_{2-y}(\text{Mn,Zn})_4\text{As}_4 \cdot n(RE\text{As})$, presented here, and $RE(\text{Mn,Zn})_{2-x}\text{As}_2 \cdot n(RE\text{As})$, reported previously.[18] Similarly, the known phases $RE_{2-y}(\text{Mn,Zn})_4\text{As}_4$ (*RE* = La–Nd, Sm–Lu)[24] can be considered to be the n = 0 members of these more complicated Mn-containing homologous series.

Like the previously known arsenides $RE\text{Zn}_{2-x}\text{As}_2 \cdot n(RE\text{As})$, the new arsenides $RE_{2-y}Zn_4As_4 \cdot n(RE\text{As})$ were obtained by reactions of the elements at 750 °C with loading compositions matching the formulas determined from single-crystal structure determinations. In contrast to $RE\text{Zn}_{2-x}\text{As}_2 \cdot n(RE\text{As})$, which could generally be prepared with high phase purity (>80%),[18] $RE_{2-y}Zn_4As_4 \cdot n(RE\text{As})$ phases were always found in conjunction with other phases and their proportions become lower on progressing to later *RE* components (Figs. S1–S3 in ESI†). Numerous attempts were made to adjust the stoichiometry (e.g., addition of up to 5% excess *RE* or up to 10% excess As), temperature (e.g., increase to 800 °C or to 900 °C), and duration of the

reactions but they did not improve phase purity significantly. These phases may well have limited stability within narrow temperature ranges or exhibit complex equilibria that remain to be clarified. The cell parameters of $RE_{2-y}Zn_4As_4 \cdot n(RE\text{As})$ refined from the powder XRD patterns show some irregular trends (Table 1), likely attributable to variability in the *RE* deficiencies (which are undetermined). In general, however, the unit cell volumes do decrease monotonically in accordance with the lanthanide contraction on progressing to smaller *RE* components. These phases adopt trigonal structures in space group $R\bar{3}m1$ with $Z = 3$ for $RE_{4-y}Zn_4As_6$ and $RE_{6-y}Zn_4As_8$, or space group $P\bar{3}m1$ with $Z = 1$ for $RE_{5-y}Zn_4As_7$. The tripling of the unit cell in $RE_{4-y}Zn_4As_6$ and $RE_{6-y}Zn_4As_8$ arises from a tripling of the *c*-parameter relative to that in $RE_{5-y}Zn_4As_7$. The trends in cell parameters are best seen by comparing the cell volume per formula unit (f.u.), *V*/*Z*, and the reduced *c*-parameter, *c*/*Z*, among these series (Fig. 1). For every increment of *n* in $RE_{2-y}Zn_4As_4 \cdot n(RE\text{As})$, the normalized cell volume increases by about 50 $Å^3$ and the reduced *c*-parameter increases by 3.3–3.4 Å, while the *a*-parameter remains constant at 4.2 Å, a manifestation of clear structural regularity as described further below.

To describe the trigonal crystal structures of the all-Zn-containing arsenides $RE_{2-y}Zn_4As_4 \cdot n(RE\text{As})$ and the Mn-doped arsenides $RE_{2-y}(Mn,Zn)_4As_4 \cdot n(RE\text{As})$ together, we combine the formulas as $RE_{2-y}M_4As_4 \cdot n(RE\text{As})$, in which *M* represents the sites occupied by Zn or Mn atoms. We first consider the $n = 2$ member of the homologous series having a hypothetical idealized formula that is fully stoichiometric, $RE_4M_4As_6$. Because the *c*-parameter is very long (62 Å), it is helpful to examine just a part of the structure at the outset (Fig. 2a). The structure is built up by condensing two types of slabs, [*RE*As] constructed from edge-sharing *RE*-centred octahedra and $[M_2As_2]$ constructed from edge-sharing *M*-centred tetrahedra, which are stacked along the *c*-direction. Equivalently, the structure consists of an arrangement of close-packed nets

of As atoms, with 2/3 of the octahedral interstices occupied by *RE* atoms and 1/3 of the tetrahedral interstices by *M* atoms. The [*RE*As] slabs are fragments of the rocksalt (NaCl-type) structure, which is adopted by the binary rare-earth monoarsenides *RE*As themselves.[28,29] The [M_2As_2] slabs are the same as the anionic substructure of the $CaAl_2Si_2$-type structure adopted by the parent $n = 0$ member of the homologous series.[15,19–21] The slabs are intergrown following the repeating sequence [*RE*As]$_3$–[M_2As_2]–[*RE*As]–[M_2As_2]–…, in which there are single-slab [*RE*As] or triple-slab [*RE*As]$_3$ blocks. The characteristic feature is the presence of "sandwiches" [M_2As_2]–[*RE*As]–[M_2As_2] that interrupt the regular rocksalt-type arrangement of *RE*As. On proceeding from the idealized structure $RE_4M_4As_6$ to the true structure $RE_{4-y}M_4As_6$, two complications arise. First, there are *RE* deficiencies, and the partially filled *RE* sites (labeled here as *RE*2) are always found in the isolated [*RE*As] slab inside the sandwiches. The occupancy is typically 0.3–0.4 in these deficient *RE* sites. Second, as a result of the space liberated by these *RE* deficiencies, a secondary metal site (labeled as *M*1b) appears which is split off from the main metal site (labeled as *M*1a) found in the inner sides of the [M_2As_2] slabs of the sandwiches (Fig. 2b). The occupancy is typically 0.7–0.8 in the primary metal sites and 0.2–0.3 in the secondary sites. On a local level, if the secondary metal site *M*1b is occupied, the adjacent *RE* site is empty in the slab inside the sandwiches; if instead the primary metal site *M*1a is occupied, the *RE* site can be filled. In Mn-doped derivatives, such as $Ce_{3.3}Mn_{1.1}Zn_{2.9}As_6$, there is a preference for Mn atoms to occupy the secondary site (*M*1b) while the Zn atoms occupy the primary site (*M*1a); the unsplit site (*M*2) is generally preferred by Zn atoms. The full structure of $RE_{4-y}M_4As_6$ can now be appreciated in both ball-and-stick and polyhedral representations (Fig. 3).

The evolution of the homologous series $RE_{2-y}M_4As_4 \cdot n$(*RE*As) is shown in Fig. 4. The parent $n = 0$ member $RE_{2-y}M_4As_4$, which is fully stoichiometric when *RE* is divalent ($EuZn_2As_2$,

$YbZn_2As_2$)[19–21] but substoichiometric when *RE* is trivalent ($RE_{0.67}Zn_2As_2$),[15] adopts the $CaAl_2Si_2$-type structure having a simple *hcp* stacking sequence (AB) of As nets and constructed from alternating [*RE*As] and [M_2As_2] slabs. For every increment in *n*, the intervening rocksalt-type blocks between the [M_2As_2]–[*RE*As]–[M_2As_2] sandwiches increase in thickness by one; this corresponds to a lengthening of the reduced *c*-parameter by 3.3–3.4 Å, noted earlier. The $n = 1$ member is unknown but would have the formula $RE_{3-y}M_4As_5$. The $n = 2$ member is $RE_{4-y}M_4As_6$ described above, having a long stacking sequence (ABABABCACACABCBCBC) of 18 As nets. These stacking sequences can be expressed in more compact notation, by identifying nets as being surrounded in hexagonal vs. cubic arrangements (e.g., *h* = A<u>B</u>A; *c* = A<u>B</u>C), or by simply specifying the lattice (*H* vs. *R*) and the number of layers present.[30] For $RE_{4-y}M_4As_6$, the stacking sequence is thus h^4c^2 (= *hhhhcc*) or 18*R*. As summarized in Table 4, each increment in *n* adds a new layer in cubic stacking sequence (*c*). Depending on the repeat length of the sequence, the space group is either $P\bar{3}m1$ ($Z = 1$) and $R\bar{3}m1$ ($Z = 3$). The *c*-parameters, which can be estimated from an increase of 3.3 Å for every additional [*RE*As] slab, agree well with observations. Experimentally, we have determined the structures of the higher members $RE_{5-y}M_4As_7$ ($n = 3$) and $RE_{6-y}M_4As_8$ ($n = 4$), the latter having a very long *c*-parameter of 82 Å.

Through the same structural principle of increasing the number of [*RE*As] slabs, the parent $n = 0$ member, REM_2As_2 or $RE_{2-y}M_4As_4$, bifurcates into metal-deficient $REM_{2-x}As_2{\cdot}n$(*RE*As) and rare-earth-deficient $RE_{2-y}M_4As_4{\cdot}n$(*RE*As) homologous series (Fig. 5). There are some interesting points worth noting in comparing members of these two series. The lower members ($RE_2M_{2-x}As_3$ and $RE_3M_{2-x}As_4$ of the first series; $RE_{3-y}M_4As_5$ of the second series) are missing and to date we have not been successful in preparing them, at least with early *RE* components. (The existence of fully stoichiometric $Eu_2Zn_2As_3$ has been reported but it adopts an

unrelated monoclinic structure.[22]) If only the ideal formulas are considered, each member of the first series necessarily has a compositionally identical counterpart with an even-numbered member of the second series. For example, doubling the fully stoichiometric formula $RE_2M_2As_3$, which is the n = 1 member in the first series, gives $RE_4M_4As_6$, which is the same formula as the n = 2 member in the second series. They have the same number of [*RE*As] slabs, which are distributed evenly (2–2–…) in $RE_2M_2As_3$ and unevenly (1–3–…) in $RE_4M_4As_6$. However, in practice, their compositions can be distinguished because of the occurrence of significant deficiencies in the *M* or *RE* sites, respectively. There are also members from the two homologous series which, by virtue of having equal numbers of repeating As layers, share nearly identical cell parameters and crystallize in the same space group. For example, although the stacking sequence differs in $RE_5M_{2-x}As_6$ (h^2c^4) in the first homologous series and $RE_{4-y}M_4As_6$ (h^4c^2) in the second homologous series, they have the same number of As nets (18*R*) in space group $R\bar{3}m1$ (compare the structures shown in Fig. 5). Thus, it can be very difficult to distinguish between them experimentally from their cell parameters alone (cf., a = 4.246(3) Å, c = 62.49(5) Å for $Pr_5Zn_{1.7}As_6$;[18] a = 4.2067(7) Å, c = 62.637(10) Å for $Pr_{3.5}Zn_4As_6$).

In both homologous series of arsenides, the absence of homoatomic bonding (metal-metal or As–As) implies that all atoms have closed-shell (d^0; RE^{3+}, As^{3-}), closed-subshell (d^{10}; Zn^{2+}), or half-filled-subshell (d^5; Mn^{2+}) configurations. Given these assignments, the fully stoichiometric formulas of these arsenides would be electron-excessive: $(RE^{3+})(M^{2+})_2(As^{3-})_2e^-\cdot n(RE^{3+}As^{3-})$ for the first homologous series, and $(RE^{3+})_2(M^{2+})_4(As^{3-})_4(e^-)_2\cdot n(RE^{3+}As^{3-})$ for the second homologous series. The electron excess can be removed through deficiencies in the *M* site, $REM_{2-x}As_2\cdot n(REAs)$, or in the *RE* site, $RE_{2-y}M_4As_4\cdot n(REAs)$. The actual formulas are $REM_{1.7-1.8}As_2\cdot n(REAs)$ and $RE_{1.3-1.4}M_4As_4\cdot n(REAs)$, which indicate that the deficiencies do not

have to be quite as low as in the strictly valence-precise formulations, $(RE^{3+})(M^{2+})_{1.5}(As^{3-})_2 \cdot n(RE^{3+}As^{3-})$ and $(RE^{3+})_{1.33}(M^{2+})_4(As^{3-})_4 \cdot n(RE^{3+}As^{3-})$, respectively. The small discrepancy between the predicted and actual deficiencies may suggest the existence of a slight homogeneity range, which would be possible especially if there is no band gap in the density of states (see later). The question of which site accommodates the deficiencies, *RE* or *M*, is an interesting one which we attempt to address below.

The occurrence of vacancies entails changes in both enthalpy and entropy terms for the free energy of a substoichiometric phase relative to the hypothetical fully stoichiometric one.[31] In general, it might be thought that removing an atom from a structure is unfavourable from an enthalpy standpoint because of the loss of bonding interactions. However, even at 0 K, low concentrations of vacancies result in a gain in entropy that can offset the cost of creating these defects. Of course, the conventional treatment of defects applies to very small deviations from ideal stoichiometry, not the significant deviations seen here in these arsenides. However, we can make use of similar ideas to construct a qualitative argument. Previous analysis of the electronic structure of $La_4Zn_2As_5$ (a member of the first homologous series) revealed that removal of electrons from the fully stoichiometric structure depopulates weakly antibonding La–As and Zn–As states so that the Fermi level is lowered to a pseuodgap.[18] In other words, a possible driving force is the optimization of bonding, with the formation of deficiencies enthalpically favoured up to a certain point; because there is considerable delocalization of the bonding electrons, however, we gain no insight as to whether La or Zn sites prefer to be deficient. We consider now the entropy changes, which have two parts: a configurational term, which depends on the distribution of vacancies and atoms within a given site, and a vibrational (or thermal) term, which depends on the bond distortions experienced by neighbouring atoms surrounding a

vacancy. Given that these arsenides were formed at ~1000 K rather than ~0 K, these entropy terms are undoubtedly important contributions to their stability. The configurational entropy favours deficiency in the lower valent site than in the higher valent site because more vacancies can be created for the same electron excess to be removed. Thus, the default response is for the M^{2+} sites rather than the RE^{3+} sites to be deficient. The vibrational entropy favours deficiency in the site with the higher coordination number (CN) than with the lower one because greater disruption of the surrounding atoms can take place. However, this is not simply a matter of comparing the coordination of As atoms surrounding *RE* (CN6) vs. *M* (CN4). To include any eventual *RE*–*M* or *M*–*M* contacts, it seems more appropriate to set a cutoff of ~3.6 Å to define the CN around a given *RE* or *M* site.

In the first homologous series, $REM_{2-x}As_2{\cdot}n(RE\text{As})$, the *RE* sites have CN6–9 (consisting of 6 As atoms and 0–3 *M* atoms) whereas the *M* sites have CN10 (consisting of 4 As, 3 *RE*, and 3 *M* atoms). Thus, both configurational and vibrational entropy favour deficiency in the *M* sites, consistent with observations. In the second homologous series, $RE_{2-y}M_4As_4{\cdot}n(RE\text{As})$, the *RE* sites have CN6–12 (consisting of 6 As atoms and 0–6 *M* atoms) whereas the *M* sites have CN10 (consisting of 4 As, 3 *RE*, and 3 *M* atoms). The key difference is that the *RE* sites sandwiched between the $[M_2As_2]$ slabs have an especially high CN of 12; the occurrence of vacancies in these *RE* sites may then confer greater vibrational entropy, enough to overcome the normal preference for Zn deficiencies. Note that in the parent $n = 0$ member common to both homologous series, the *RE* atoms are always sandwiched between $[M_2As_2]$ slabs; consequently, for trivalent *RE* components, $RE_{0.67}Zn_2As_2$ are also deficient in *RE*. The occurrence of a split *M* site that enters the liberated space of a *RE* vacancy in the structures of $RE_{2-y}M_4As_4{\cdot}n(RE\text{As})$ is a manifestation of the significant bond relaxation that takes place, and this feature has the benefit

of contributing additional configurational entropy. Note that the reverse – split *RE* sites within the space vacated by a Zn deficiency – cannot happen because *RE* atoms are too big to enter into the Zn-containing slabs.

The electronic band structures of members within the homologous series are expected to vary gradually as more [*RE*As] slabs are introduced. A calculation was first performed on a fully stoichiometric model of an intermediate member (n = 2), with the idealized formula $La_4Zn_4As_6$. The density of states (DOS) curve shows a broad valence band (from –7 to –1 eV) that is separated by a small gap of 0.04 eV from a conduction band extending upwards in energy (Fig. 6). Consistent with the electron excess implied by this formula, $(La^{3+})_4(Zn^{2+})_4(As^{3-})_6(e^-)_2$, the Fermi level cuts through the bottom of the conduction band. Removal of exactly two electrons per formula unit lowers the Fermi level to where the band gap is located, corresponding to the valence-precise formulation $(La^{3+})_{3.3}(Zn^{2+})_4(As^{3-})_6$ in which the electron excess is assumed to be alleviated through *RE* deficiencies. At first glance, the closed shell or subshell configurations are generally supported by the occurrence of mostly empty La-based states found above the Fermi level, and mostly filled Zn- and As-based states below. The narrow completely filled Zn 3d-band is centred at –8.6 eV. The As-based states occur as two separate 4s bands (near –10 and –12 eV) and a wide manifold of 4p states within the valence band. However, there is considerable mixing of states from all three atoms in the valence band. In particular, the substantial contribution of La-based states here implies that, contrary to the usual assumption that La atoms mainly participate in ionic interactions, the role of covalent bonding is also important. In fact, as seen in the crystal orbital Hamilton population (COHP) curves (Fig. 6), the La–As covalent bonding interactions are quite significant when compared to the Zn–As interactions. Both types of bonding are optimized when the Fermi level is located at the gap at –1 eV, resulting in

integrated COHP values (–ICOHP) of 0.76 eV/bond for La–As and 1.49 eV/bond for Zn–As interactions. Above this gap, the interactions are nonbonding for La–As or very weakly antibonding for Zn–As interactions. From this point of view, it may be thought that depopulation of the Zn–As antibonding states favours the occurrence of Zn deficiences, but as discussed above, entropy stabilization may favour the occurrence for *RE* deficiencies instead. Interestingly, of the three La sites in this structural model, the one sandwiched between the $[Zn_2As_2]$ slabs (labeled as *RE*2 in Fig. 2) participates in the weakest La–As bonds (–ICOHP of 0.63 eV/bond) compared to the other two (–ICOHP of 0.90 and 0.74 eV/bond), despite nearly identical bond lengths of 3.0 Å. Thus, this site should be the least energetically costly one for vacancies to be created (accompanied by the loss of La–As bonding interactions), in agreement with observations.

Extrapolation to other members of the homologous series with idealized fully stoichiometric formulas $La_2Zn_4As_4 \cdot n(LaAs)$ (n = 0, 1, 2, 3, 4, 5, and ∞) shows clear trends in the DOS curves (Fig. 7). The calculations were performed on models with real counterparts (n = 0, 2, 3, 4, ∞) or based on hypothetical structures (n = 1, 5). As n increases, the effect of increasing the number of [*RE*As] slabs is to narrow the gap between valence and conduction bands. The gap starts off at 0.60 eV in the parent n = 0 member ($La_2Zn_4As_4$) and gradually narrows to 0.04 eV at n = 2 ($La_4Zn_4As_6$); beyond this point, the valence and conduction bands just touch at a pseudogap with low DOS (e.g. 0.5 states/eV·cell in $La_5Zn_4As_7$). Lowering the Fermi level to the gap or pseudogap, through removal of two electrons per formula unit, leads to valence-precise formulations consistent with the *RE* deficiencies observed in the ternary arsenides. The DOS curves show that the electronic structure is derived from a superposition of [*RE*As] and $[Zn_2As_2]$ slabs. Because the number of $[Zn_2As_2]$ slabs is constant in the homologous series, the

projections of states originating from them also remains unchanged. Adding more [*RE*As] slabs increases the proportion of states originating from isolated As atoms which are partitioned into lower energy 4s (near –10 eV) and higher energy 4p bands (from –4 to –1 eV). In the limit reached in LaAs ($n = \infty$), the DOS curve corresponds essentially to filled As states and empty La states, consistent with the simple formulation $La^{3+}As^{3-}$. However, even here, there is still substantial mixing of La 5d states with As 4p states, implying that La–As interactions have considerable covalent character. In both this rare-earth-deficient series $RE_{2-y}M_4As_4{\cdot}n(RE\text{As})$ and the previously known metal-deficient series $REM_{2-x}As_2{\cdot}n(RE\text{As})$, the transition from a small band gap semiconductor, characteristic of $CaAl_2Si_2$-type phases like the parent $n = 0$ members, to a semimetal, in the limit of LaAs, occurs when the number of [*RE*As] slabs is four or more.

Conclusions

The homologous series $RE_{2-y}Zn_4As_4{\cdot}n(RE\text{As})$ illustrates the remarkable diversity of structures that can be built by intergrowing [*RE*As] and $[Zn_2As_2]$ slabs. As in the previously known series $REZn_{2-x}As_2{\cdot}n(RE\text{As})$ made of the same types of slabs, higher members are derived by condensing [*RE*As] slabs into thicker blocks, which causes a narrowing of the gap between valence and conduction bands until they eventually just touch to give semimetallic behaviour. In both cases, the formation of vacancies relieves the electron excess that would be found in the fully stoichiometric formulas. Enthalpy factors normally favour Zn defects, as found in $REZn_{2-x}As_2{\cdot}n(RE\text{As})$, because weakly antibonding Zn–As states can be depopulated. On the other hand, in $RE_{2-y}Zn_4As_4{\cdot}n(RE\text{As})$, the characteristic feature of single [*RE*As] slabs sandwiched between $[Zn_2As_2]$ slabs leads to particularly high CN of these *RE* sites, within which formation of defects can provide entropic stabilization. As an alternative to condensing [*RE*As] slabs, it is possible to

imagine that related homologous series could be built up by condensing $[Zn_2As_2]$ slabs instead. In such a scenario, the metal sites with the highest CN would be found among the innermost Zn sites of condensed $[Zn_2As_2]$ blocks. Synthesis of targeted compounds within this hypothetical homologous series has so far been challenging because the formulas would be identical to members found in other series; in other words, these polymorphic forms, if they existed, would likely need to be prepared under different temperature conditions. For example, one hypothetical structure with condensed $[Zn_2As_2]$ slabs would have the idealized formula $RE_5Zn_4As_7$, which is identical to the $n = 3$ member of the $RE_{2-y}Zn_4As_4 \cdot n(RE\text{As})$ series. Reassuringly, we do have preliminary evidence for the formation of $Gd_5Zn_{4-x}As_7$, in which the structure contains a pair of condensed $[Zn_2As_2]$ slabs with deficiences in the interior Zn sites, in agreement with predictions.

Acknowledgements

This work was supported by the Natural Sciences and Engineering Research Council of Canada (NSERC).

References

1 M. Jansen and J. C. Schön, *Angew. Chem. Int. Ed.*, 2006, **45**, 3406–3412.

2 M. G. Kanatzidis, *Acc. Chem. Res.*, 2005, **38**, 361–370.

3 P. F. P. Poudeu and M. G. Kanatzidis, *Chem. Commun.*, 2005, 2672–2674.

4 S. E. Latturner and M. G. Kanatzidis, *Inorg. Chem.*, 2008, **47**, 2089–2097.

5 A. M. Abakumov, J. Hadermann, M. Batuk, H. D'Hondt, O. A. Tyablikov, M. G. Rozova, K. V. Pokholok, D. S. Filimonov, D. V. Sheptyakov, A. A. Tsirlin, D. Niermann, J. Hemberger, G. van Tendeloo and E. V. Antipov, *Inorg. Chem.*, 2010, **49**, 9508–9516.

6 C. M. Ainsworth, C.-H. Wang, H. E. Johnston, E. E. McCabe, M. G. Tucker, H. E. A. Brand and J. S. O. Evans, *Inorg. Chem.*, 2015, **54**, 7230–7238.

7 A. Mrotzek and M. G. Kanatzidis, *Acc. Chem. Res.*, 2003, **36**, 111–119.

8 M. Ruck and P. F. P. Poudeu, *Z. Anorg. Allg. Chem.*, 2008, **634**, 482–490.

9 T.-S. You, P. H. Tobash and S. Bobev, *Inorg. Chem.*, 2010, **49**, 1773–1783.

10 M. Karpinnen and H. Yamauchi, in *Frontiers in Superconducting Materials*, ed. A. V. Narlikar, Springer-Verlag, Berlin, 2005, pp. 255–294.

11 Z. A. Gál, O. J. Rutt, C. F. Smura, T. P. Overton, N. Barrier, S. J. Clarke and J. Hadermann, *J. Am. Chem. Soc.*, 2006, **128**, 8530–8540.

12 H. Ogino, K. Machida, A. Yamamoto, K. Kishio, J. Shimoyama, T. Tohei and Y. Ikuhara, *Supercond. Sci. Technol.*, 2010, **23**, 115005-1–115005-5.

13 A. T. Nientiedt and W. Jeitschko, *J. Solid State Chem.*, 1999, **142**, 266–272.

14 S. S. Stoyko and A. Mar, *J. Solid State Chem.*, 2011, **184**, 2360–2367.

15 A. T. Nientiedt, H. Lincke, U. Ch. Rodewald, R. Pöttgen and W. Jeitschko, *Z. Naturforsch. B: J. Chem. Sci.*, 2011, **66**, 221–226.

16 S. S. Stoyko and A. Mar, *Inorg. Chem.*, 2011, **50**, 11152–11161.

17 X. Lin, S. S. Stoyko and A. Mar, *J. Solid State Chem.*, 2013, **199**, 189–195.

18 X. Lin and A. Mar, *Inorg. Chem.*, 2013, **52**, 7261–7270.

19 P. Klüfers, H. Neumann, A. Mewis and H.-U. Schuster, *Z. Naturforsch. B: Anorg. Chem., Org. Chem.*, 1980, **35**, 1317–1318.

20 G. Zwiener, H. Neumann and H.-U. Schuster, *Z. Naturforsch. B: Anorg. Chem., Org. Chem.*, 1981, **36**, 1195–1197.

21 A. Nateprov, J. Cisowski, J. Heimann and I. Mirebeau, *J. Alloys Compd.*, 1999, **240**, 6–9.

22 S. S. Stoyko, M. Khatun and A. Mar, *Inorg. Chem.*, 2012, **51**, 2621–2628.

23 B. Saparov and S. Bobev, *Acta Crystallogr., Sect. E: Struct. Rep. Online*, 2010, **66**, i24.

24 X. Lin, D. Tabassum, B. W. Rudyk and A. Mar, *Inorg. Chem.*, 2014, **53**, 8431–8441.

25 G. M. Sheldrick, *SHELXTL, version 6.12*, Bruker AXS Inc., Madison, WI, 2001.

26 L. M. Gelato and E. Parthé, *J. Appl. Crystallogr.*, 1987, **20**, 139–143.

27 R. Tank, O. Jepsen, A. Burkhardt and O. K. Andersen, *TB–LMTO–ASA Program, version 4.7*, Max Planck Institut für Festkörperforschung, Stuttgart, 1998.

28 L. H. Brixner, *J. Inorg. Nucl. Chem.*, 1960, **15**, 199–201.

29 J. B. Taylor, L. D. Calvert, J. G. Despault, E. J. Gabe and J. J. Murray, *J. Less-Common Met.*, 1974, **34**, 217–232.

30 W. B. Pearson, *The Crystal Chemistry and Physics of Metals and Alloys*, Wiley, New York, 1972.

31 J. S. Anderson, in *Nonstoichiometric Compounds*, ed. R. Ward, *Advances in Chemistry,* American Chemical Society, Washington, DC, 1963, pp. 1–22.

Table 1 Cell parameters for $RE_{2-y}Zn_4As_4 \cdot n(RE\text{As})$ (n = 2, 3, 4) in powder samples obtained by reaction of the elements at 750 °C

Compound	a (Å)	c (Å)	V (Å^3)
$La_{4-y}Zn_4As_6$	4.1915(3)	62.637(6)	953.0(1)
$Ce_{4-y}Zn_4As_6$	4.1947(3)	62.267(6)	948.9(1)
$Pr_{4-y}Zn_4As_6$	4.1639(3)	62.660(6)	940.8(1)
$Nd_{4-y}Zn_4As_6$	4.1570(3)	62.065(6)	928.8(1)
$Pr_{5-y}Zn_4As_7$	4.1868(3)	24.161(1)	366.80(5)
$Nd_{5-y}Zn_4As_7$	4.1804(3)	24.075(1)	364.36(5)
$Sm_{5-y}Zn_4As_7$	4.1842(3)	23.906(1)	362.47(5)
$Gd_{5-y}Zn_4As_7$	4.1710(3)	23.925(1)	360.47(5)
$La_{6-y}Zn_4As_8$	4.2001(2)	83.028(6)	1268.5(1)
$Ce_{6-y}Zn_4As_8$	4.1990(2)	82.863(6)	1265.2(1)
$Pr_{6-y}Zn_4As_8$	4.1956(2)	82.113(6)	1251.8(1)
$Nd_{6-y}Zn_4As_8$	4.1700(2)	81.990(6)	1234.7(1)
$Sm_{6-y}Zn_4As_8$	4.1662(2)	81.877(6)	1230.7(1)
$Gd_{6-y}Zn_4As_8$	4.1637(2)	81.747(6)	1227.3(1)

Table 2 Abbreviated crystallographic data for $RE_{2-y}Mn_xZn_{4-x}As_4 \cdot n(RE\text{As})$ (n = 2, 3, 4) [a]

Formula	fw (amu)	Space group	Z	a (Å)	c (Å)	V (Å^3)	ρ_c (g cm^{-3})	μ (mm^{-1})	$R(F)$ [b]	$R_w(F_o^2)$ [c]
$Ce_{3.32(1)}Mn_{1.1(1)}Zn_{2.9(1)}As_6$	1162.27	$R\bar{3}m1$	3	4.218(3)	62.11(4)	957.0(13)	6.050	33.34	0.032	0.058
$Pr_{3.46(1)}Zn_4As_6$	1197.14	$R\bar{3}m1$	3	4.2067(7)	62.637(10)	959.9(4)	6.213	35.57	0.021	0.045
$Nd_{3.34(1)}Mn_{0.92(6)}Zn_{3.08(6)}As_6$	1182.07	$R\bar{3}m1$	3	4.1788(7)	61.727(10)	933.5(3)	6.308	36.14	0.026	0.056
$Nd_{4.41(1)}Zn_4As_7$	1420.58	$P\bar{3}m1$	1	4.197(3)	24.204(15)	369.2(5)	6.390	37.49	0.029	0.051
$Sm_{4.39(1)}Zn_4As_7$	1447.46	$P\bar{3}m1$	1	4.1703(6)	23.981(3)	361.19(12)	6.654	39.96	0.028	0.067
$Nd_{5.43(1)}Zn_4As_8$	1644.54	$R\bar{3}m1$	3	4.2038(11)	82.97(2)	1269.8(7)	6.452	37.38	0.040	0.094
$Sm_{5.40(1)}Zn_4As_8$	1672.73	$R\bar{3}m1$	3	4.1689(4)	82.103(9)	1235.8(3)	6.743	40.53	0.026	0.053
$Sm_{5.33(1)}Mn_{0.58(1)}Zn_{3.42(1)}As_8$	1656.80	$R\bar{3}m1$	3	4.1691(9)	81.965(17)	1233.8(6)	6.690	39.97	0.025	0.053
$Gd_{5.27(1)}Mn_{0.62(1)}Zn_{3.38(1)}As_8$	1682.59	$R\bar{3}m1$	3	4.1398(12)	81.17(2)	1204.8(8)	6.957	43.15	0.033	0.088

[a] For all structures, T = 296(2) K, λ = 0.71073 Å. [b] $R(F) = \sum||F_o| - |F_c|| / \sum|F_o|$ for $F_o^2 > 2\sigma(F_o^2)$. [c] $R_w(F_o^2) = [\sum[w(F_o^2 - F_c^2)^2] / \sum wF_o^4]^{1/2}$; $w^{-1} = [\sigma^2(F_o^2) + (Ap)^2 + Bp]$, where $p = [\max(F_o^2,0) + 2F_c^2] / 3$.

Table 3 Ranges of interatomic distances (Å) for $RE_{2-y}Mn_xZn_{4-x}As_4 \cdot n(RE\text{As})$ (n = 2, 3, 4)

	$Ce_{3.32(1)}Mn_{1.1(1)}Zn_{2.9(1)}As_6$	$Pr_{3.46(1)}Zn_4As_6$	$Nd_{3.34(1)}Mn_{0.92(6)}Zn_{3.08(6)}As_6$	
*RE*1–As (CN6)	2.991(2)–3.067(2)	2.970(1)–3.050(1)	2.952(1)–3.012(1)	
*RE*2–As (CN6)	2.901(2)	2.987(1)	2.917(1)	
*RE*3–As (CN6)	3.023(2)	3.008(1)	2.978(1)	
*M*1a–As (CN4)	2.530(2)–2.698(6)	2.507(1)–2.754(2)	2.497(1)–2.755(2)	
*M*1b–As (CN4)	2.469(3)–2.747(18)	2.520(3)–2.804(10)	2.456(2)–2.817(8)	
*M*2–As (CN4)	2.529(5)–2.581(2)	2.530(2)–2.571(1)	2.515(2)–2.570(1)	
	$Nd_{4.41(1)}Zn_4As_7$	$Sm_{4.39(1)}Zn_4As_7$		
*RE*1–As (CN6)	2.977(1)–3.001(2)	2.950(1)–2.969(1)		
*RE*2–As (CN6)	2.962(2)–3.018(2)	2.938(1)–2.986(1)		
*RE*3–As (CN6)	2.969(2)	2.947(1)		
*M*1a–As (CN4)	2.490(2)–2.809(3)	2.473(1)–2.837(3)		
*M*1b–As (CN4)	2.502(3)–2.805(12)	2.487(3)–2.776(11)		
*M*2–As (CN4)	2.510(2)–2.576(2)	2.503(2)–2.570(1)		
	$Nd_{5.43(1)}Zn_4As_8$	$Sm_{5.40(1)}Zn_4As_8$	$Sm_{5.33(1)}Mn_{0.58(1)}Zn_{3.42(1)}As_8$	$Gd_{5.27(1)}Mn_{0.62(1)}Zn_{3.38(1)}As_8$
*RE*1–As (CN6)	2.970(1)–3.008(1)	2.940(1)–2.973(1)	2.942(1)–2.973(1)	2.913(1)–2.949(1)
*RE*2–As (CN6)	2.960(1)–3.025(1)	2.931(1)–2.989(1)	2.934(1)–2.989(1)	2.899(1)–2.978(1)
*RE*3–As (CN6)	2.973(1)	2.944(1)	2.917(1)	2.871(1)
*RE*4–As (CN6)	2.989(1)	2.956(1)	2.958(1)	2.931(1)
*M*1–As (CN4)	2.510(3)–2.578(1)	2.506(2)–2.565(1)	2.507(2)–2.570(1)	2.522(2)–2.558(1)
*M*2a–As (CN4)	2.496(1)–2.793(3)	2.475(1)–2.815(2)	2.488(1)–2.778(3)	2.495(1)–2.715(3)
*M*2b–As (CN4)	2.504(4)–2.818(17)	2.483(2)–2.780(10)	2.455(2)–2.811(7)	2.426(2)–2.764(9)

Table 4 Observed and predicted members of homologous series $RE_{2-y}M_4As_4{\cdot}n(RE As)$

n	idealized formula	space group	fraction of sites occupied		As stacking	c (Å)
			oct. by RE	tet. by M		
0	$RE_2M_4As_4$ [a]	$P\bar{3}m1$	2/4	2/4	h^4 (4H)	14.0
1	$RE_3M_4As_5$ [b]	$R\bar{3}m1$	3/5	2/5	h^4c (15R)	17.3 × 3 = 51.9
2	$RE_4M_4As_6$	$R\bar{3}m1$	4/6	2/6	h^4c^2 (18R)	20.7 × 3 = 62.1
3	$RE_5M_4As_7$	$P\bar{3}m1$	5/7	2/7	h^4c^3 (7H)	24.0
4	$RE_6M_4As_8$	$R\bar{3}m1$	6/8	2/8	h^4c^4 (24R)	27.4 × 3 = 82.2
5	$RE_7M_4As_9$ [b]	$R\bar{3}m1$	7/9	2/9	h^4c^5 (27R)	30.7 × 3 = 92.1

[a] For ease of comparison to the other members, this formula is doubled. [b] Hypothetical compounds.

Figure captions

Fig. 1. (a) Plots of cell volume per formula unit for different *RE* members of the three series $RE_{4-y}Zn_4As_6$, $RE_{5-y}Zn_4As_7$, and $RE_{6-y}Zn_4As_8$. (b) Plots of cell lengths as a function of *n* in the homologous series $RE_{2-y}Zn_4As_4{\cdot}n(RE\text{As})$. The *c*-parameters are normalized by dividing by 3 for structures in space group $R\bar{3}m1$.

Fig. 2. (a) A fragment of the structure of $RE_{4-y}M_4As_6$, the $n = 2$ member of $RE_{2-y}M_4As_4{\cdot}n(RE\text{As})$ (M = Mn, Zn). The *RE*2 sites (lightly shaded) are partially occupied at 0.3–0.4. Mn and Zn atoms are found in a set of split *M*1a (primary, with occupancy of 0.7–0.8, preferred by Zn) and *M*1b sites (secondary, with occupancy of 0.2–0.3, preferred by Mn), or in the unsplit M2 sites (preferred by Zn). (b) Local coordination within the $[M_2As_2]$ slab is either tetrahedral geometry exhibited by *M*1b sites or octahedral geometry by *RE*2 sites, with *M*1a sites in adjacent slabs.

Fig. 3. Full structure of $RE_{4-y}M_4As_6$, with unit cell outlined, in (a) ball-and-stick and (b) polyhedral representations, showing the intergrowth of [*RE*As] slabs built from edge-sharing octahedra and $[M_2As_2]$ slabs built from edge-sharing tetrahedra.

Fig. 4. Structures of the $n = 0$, 2, 3, and 4 members of the homologous series $RE_{2-y}M_4As_4{\cdot}n(RE\text{As})$ in terms of [*RE*As] slabs (yellow) and $[M_2As_2]$ slabs (green). The stacking sequences of As nets are also marked.

Fig. 5. Starting from the same parent member REM_2As_2 (or $RE_2M_4As_4$), inserting additional [*RE*As] slabs leads to either the metal-deficient homologous series $REM_{2-x}As_2{\cdot}n(RE\text{As})$ (left) and the rare-earth-deficient homologous series $RE_{2-y}M_4As_4{\cdot}n(RE\text{As})$ (right). Hypothetical structures have their formulas shown in parentheses.

Fig. 6. (a) Density of states (DOS) and (b) crystal orbital Hamilton population (–COHP) curves for idealized fully stoichiometric model $La_4Zn_4As_6$. Removal of two electrons per formula unit lowers the Fermi level from 0 eV (solid line) to the gap at –1 eV (dashed line).

Fig. 7. DOS curves for several members of homologous series $La_2Zn_4As_4 \cdot n$(LaAs) based on real, rare-earth-deficient compounds (n = 0, 2, 3, 4), hypothetical models (n = 1, 5), and the limiting extreme of LaAs ($n = \infty$). Regions shaded in green represent projections of states originating from $[Zn_2As_2]$ slabs; the remaining regions shaded in yellow are states originating from [LaAs] slabs. Removal of two electrons per formula unit lowers the Fermi level to energies indicated by the dashed lines.

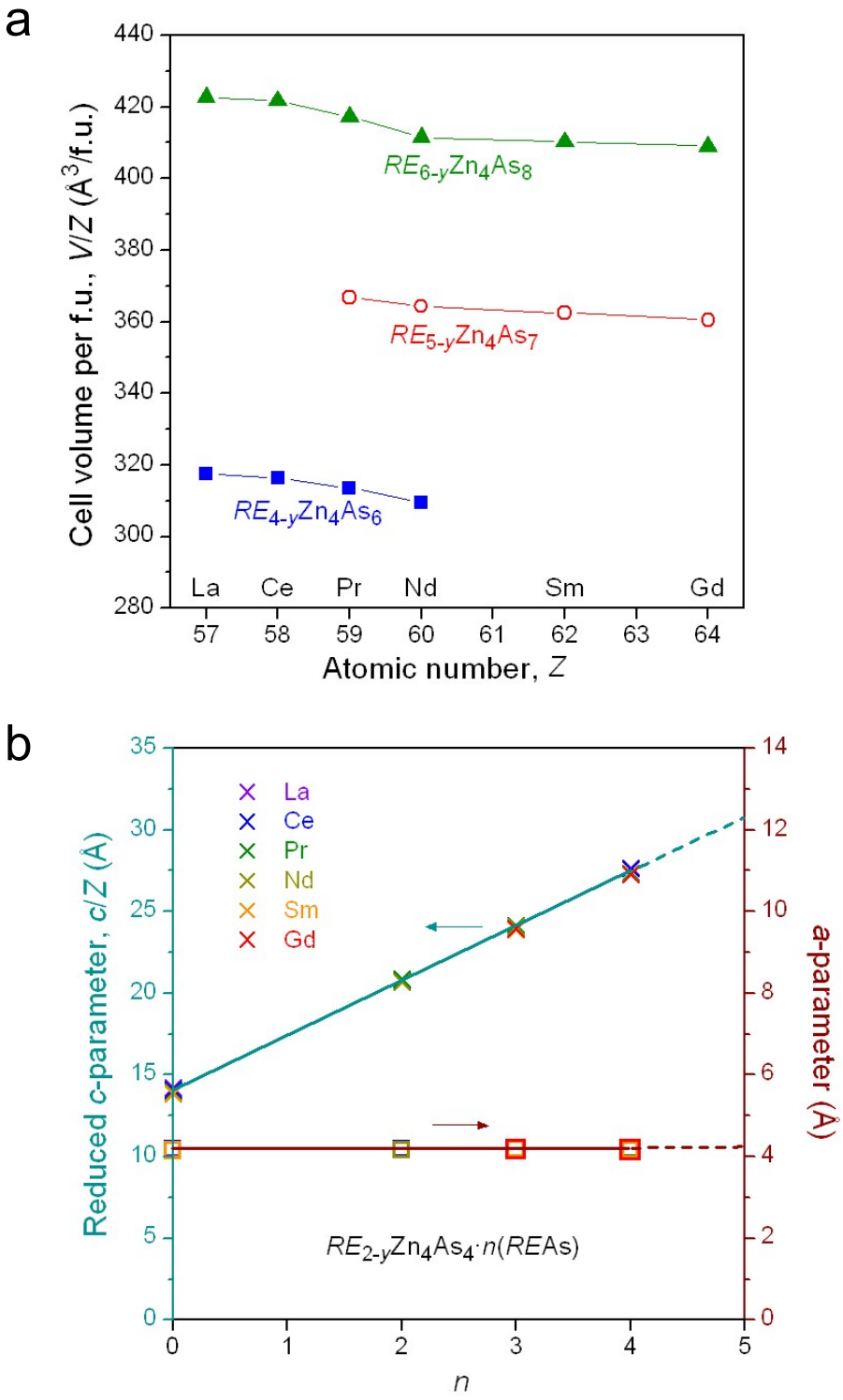

Fig. 1. (a) Plots of cell volume per formula unit for different *RE* members of the three series $RE_{4-y}Zn_4As_6$, $RE_{5-y}Zn_4As_7$, and $RE_{6-y}Zn_4As_8$. (b) Plots of cell lengths as a function of *n* in the homologous series $RE_{2-y}Zn_4As_4{\cdot}n(REAs)$. The *c*-parameters are normalized by dividing by 3 for structures in space group $R\bar{3}m1$.

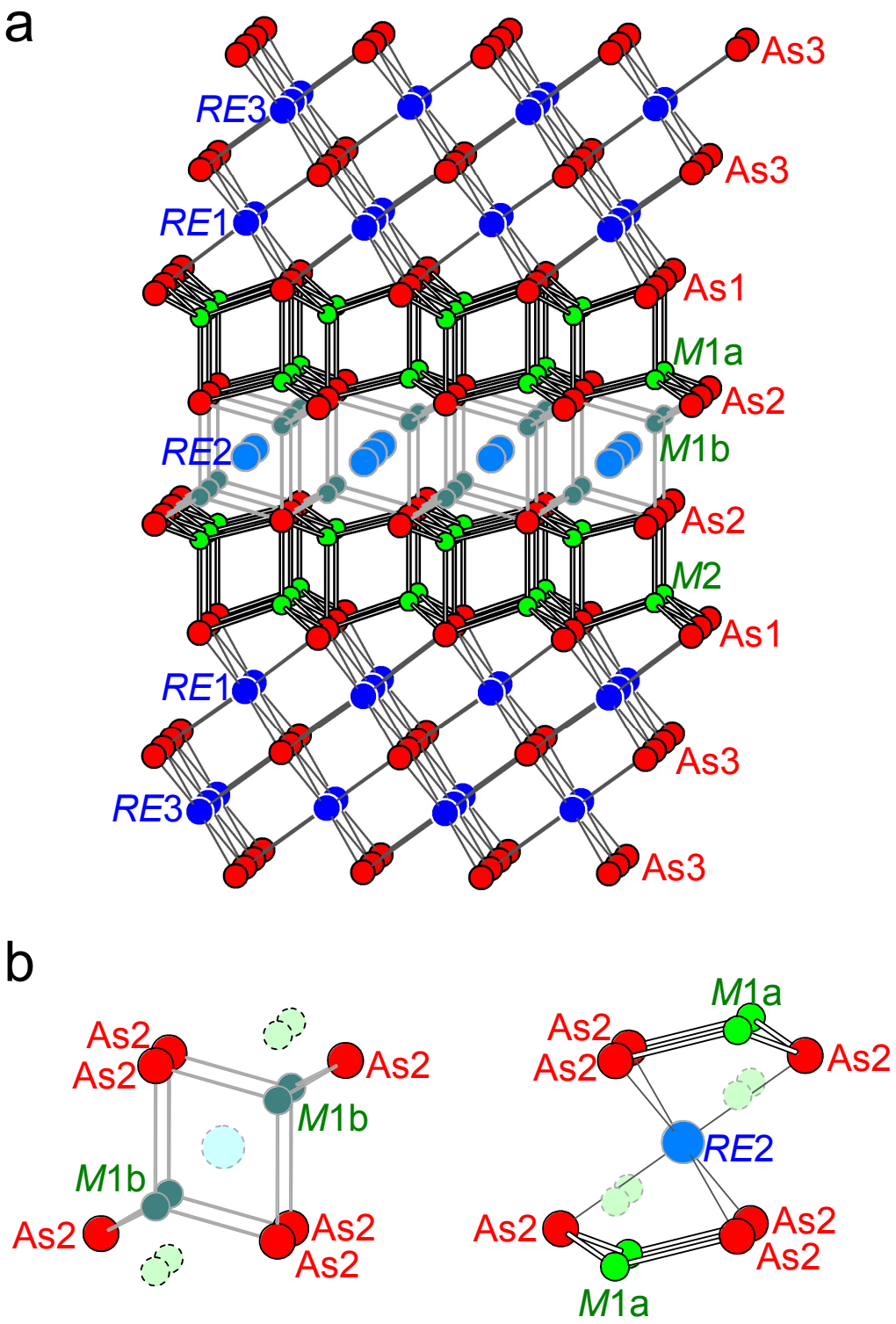

Fig. 2. (a) A fragment of the structure of $RE_{4-y}M_4As_6$, the $n = 2$ member of $RE_{2-y}M_4As_4{\cdot}n(REAs)$ (M = Mn, Zn). The *RE*2 sites (lightly shaded) are partially occupied at 0.3–0.4. Mn and Zn atoms are found in a set of split *M*1a (primary, with occupancy of 0.7–0.8, preferred by Zn) and *M*1b sites (secondary, with occupancy of 0.2–0.3, preferred by Mn), or in the unsplit M2 sites (preferred by Zn). (b) Local coordination within the $[M_2As_2]$ slab is either tetrahedral geometry exhibited by *M*1b sites or octahedral geometry by *RE*2 sites, with *M*1a sites in adjacent slabs.

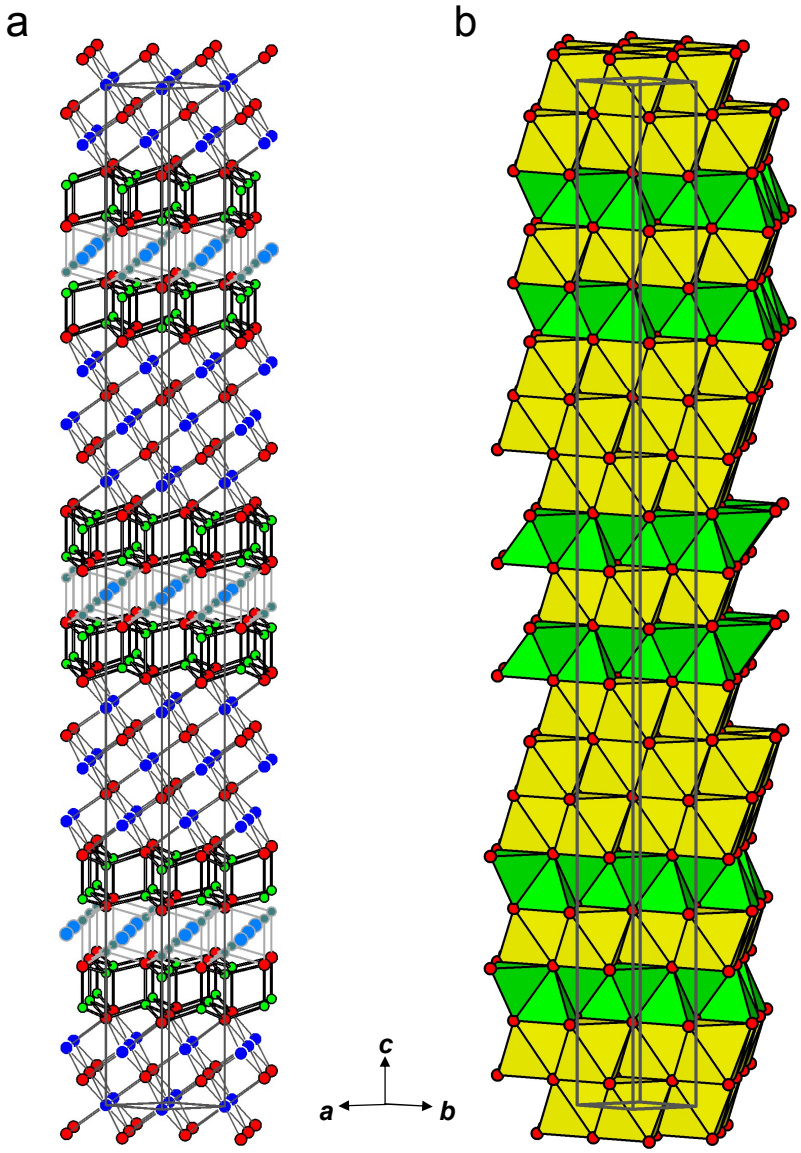

Fig. 3. Full structure of $RE_{4-y}M_4As_6$, with unit cell outlined, in (a) ball-and-stick and (b) polyhedral representations, showing the intergrowth of [*RE*As] slabs built from edge-sharing octahedra and [M_2As_2] slabs built from edge-sharing tetrahedra.

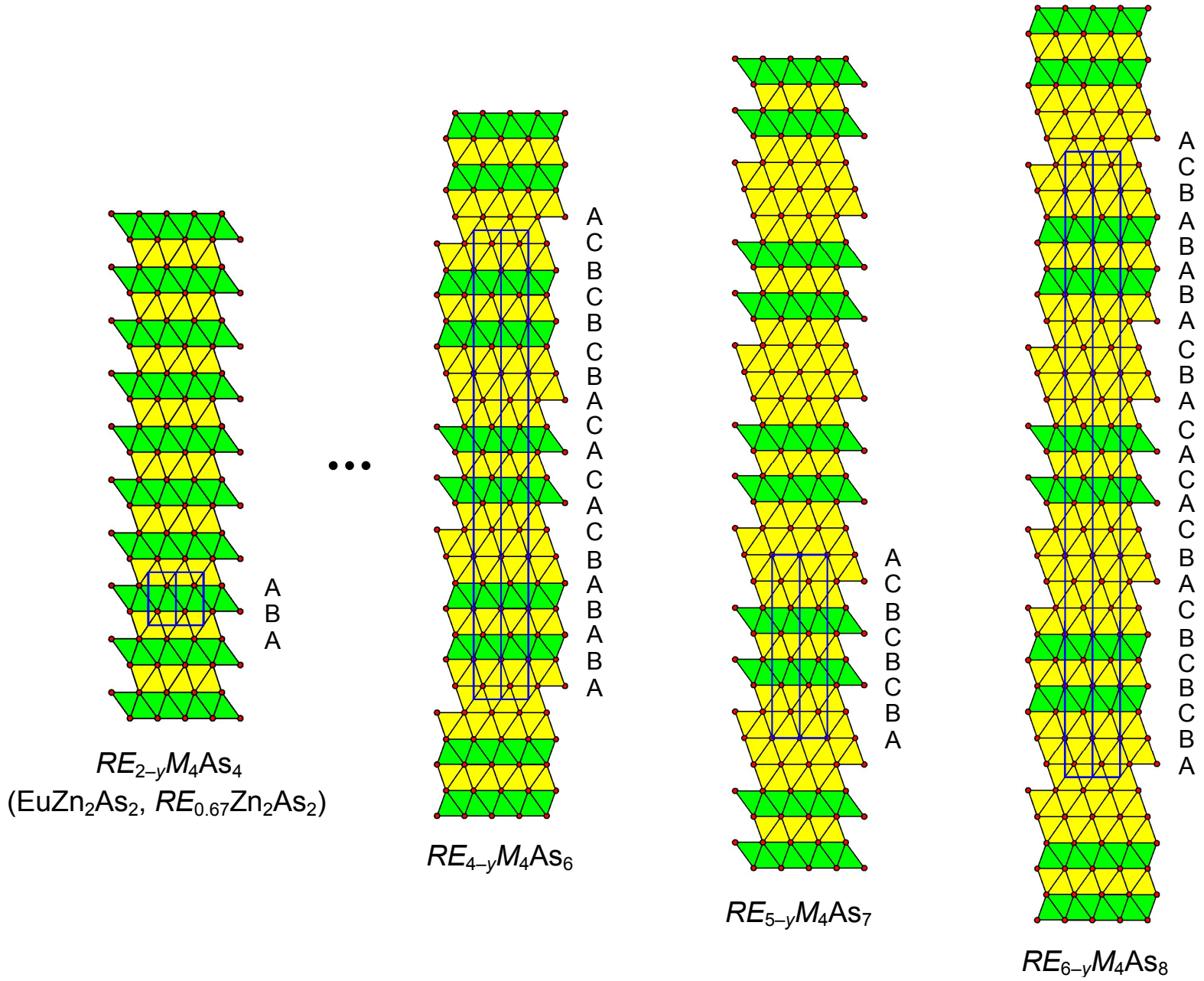

Fig. 4. Structures of the n = 0, 2, 3, and 4 members of the homologous series $RE_{2-y}M_4As_4 \cdot n(RE\text{As})$ in terms of [REAs] slabs (yellow) and [M_2As_2] slabs (green). The stacking sequences of As nets are also marked.

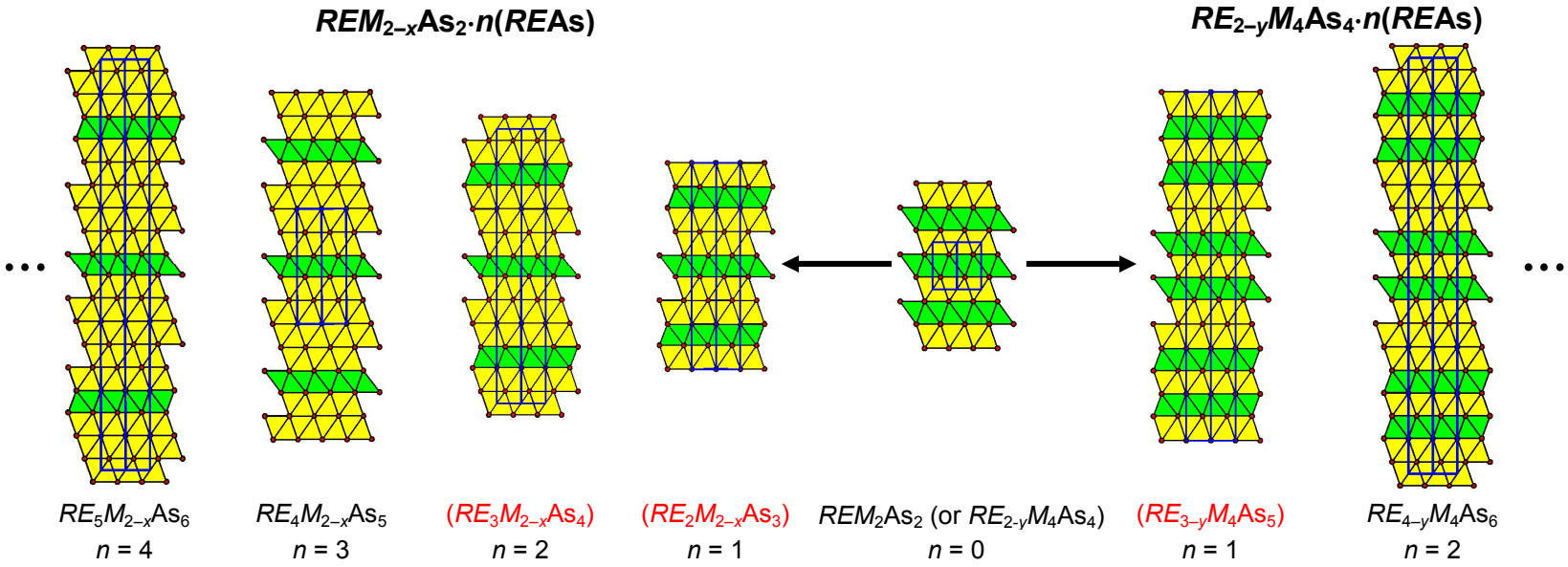

Fig. 5. Starting from the same parent member REM_2As_2 (or $RE_2M_4As_4$), inserting additional [*RE*As] slabs leads to either the metal-deficient homologous series $REM_{2-x}As_2{\cdot}n(REAs)$ (left) and the rare-earth-deficient homologous series $RE_{2-y}M_4As_4{\cdot}n(REAs)$ (right). Hypothetical structures have their formulas shown in parentheses.

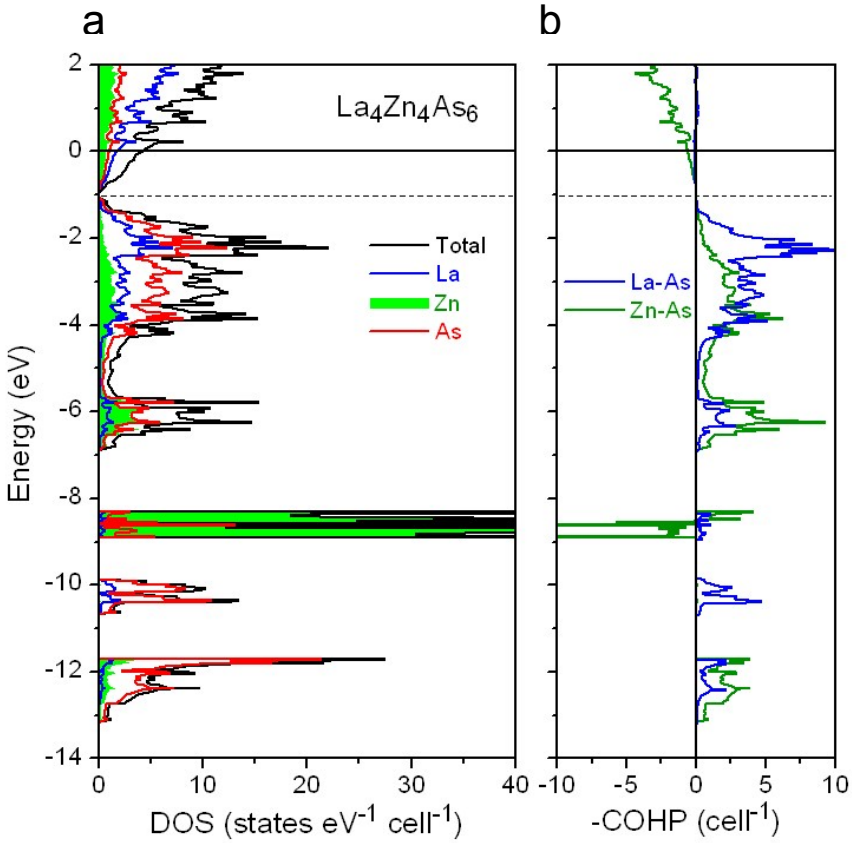

Fig. 6. (a) Density of states (DOS) and (b) crystal orbital Hamilton population (–COHP) curves for idealized fully stoichiometric model $La_4Zn_4As_6$. Removal of two electrons per formula unit lowers the Fermi level from 0 eV (solid line) to the gap at –1 eV (dashed line).

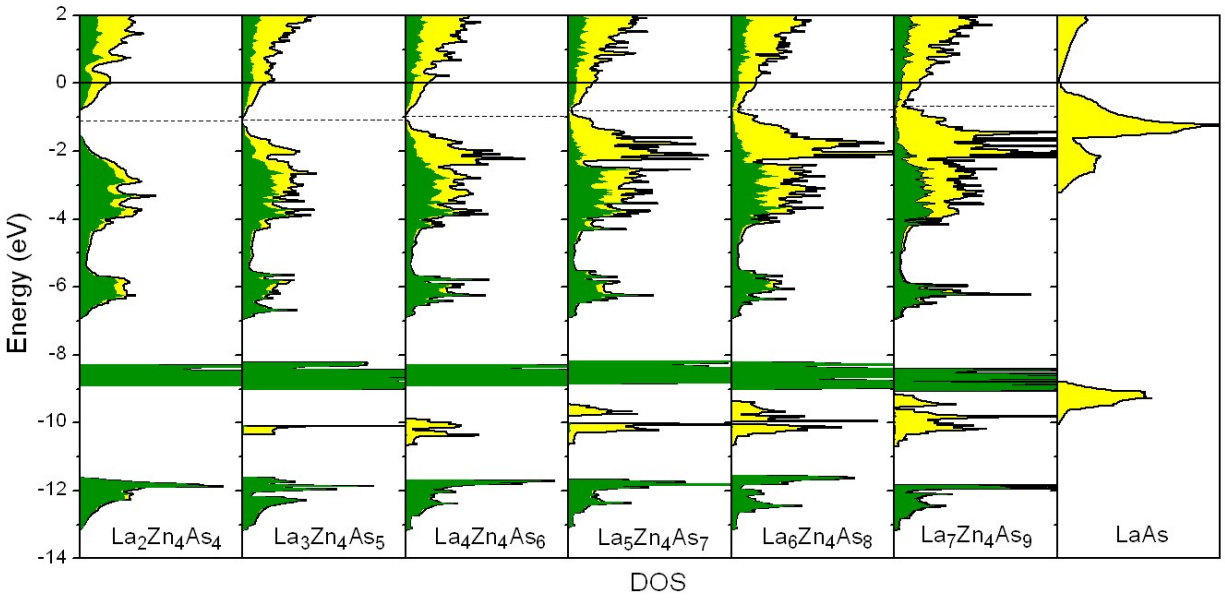

Fig. 7. DOS curves for several members of homologous series $La_2Zn_4As_4 \cdot n(LaAs)$ based on real, rare-earth-deficient compounds (n = 0, 2, 3, 4), hypothetical models (n = 1, 5), and the limiting extreme of LaAs ($n = \infty$). Regions shaded in green represent projections of states originating from $[Zn_2As_2]$ slabs; the remaining regions shaded in yellow are states originating from [LaAs] slabs. Removal of two electrons per formula unit lowers the Fermi level to energies indicated by the dashed lines.

Graphical contents entry

Narrowing the gap: From semiconductor to semimetal in the homologous series of rare-earth zinc arsenides $RE_{2-y}Zn_4As_4 \cdot n(RE\text{As})$ and Mn-substituted derivatives $RE_{2-y}Mn_xZn_{4-x}As_4 \cdot n(RE\text{As})$ (RE = La–Nd, Sm, Gd)

Xinsong Lin, Danisa Tabassum, and Arthur Mar, *Dalton Trans.*, 2015, **xx**, xxxx
DOI: 10.1039/xxxxxxxx

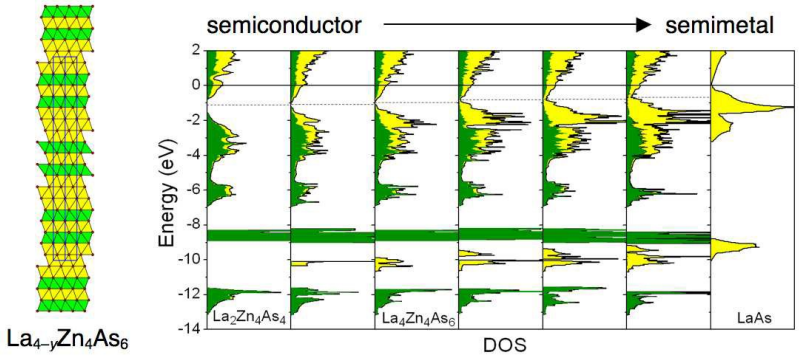

Condensing rocksalt-type [*RE*As] slabs into thicker blocks narrows the gap between valence and conduction bands within a homologous series of rare-earth-deficient ternary arsenides.